JOURNAL OF MATERIALS SCIENCE **36** (2001) 4875–4882

Hydrothermal precipitation and characterization of nanocrystalline $BaTiO_3$ particles

E. CIFTCI, M. N. RAHAMAN
Department of Ceramic Engineering, University of Missouri-Rolla, Rolla, MO 65409, USA
E-mail: rahaman@umr.edu

M. SHUMSKY
Graduate Center for Materials Research, University of Missouri-Rolla, Rolla, MO 65409, USA

Crystalline $BaTiO_3$ powders were precipitated by reacting fine TiO_2 particles with a strongly alkaline solution of $Ba(OH)_2$ under hydrothermal conditions at 80°C to 240°C. The characteristics of the powders were investigated by X-ray diffraction, transmission electron microscopy, thermal analysis and atomic emission spectroscopy. For a fixed reaction time of 24 hours, the average particle size of $BaTiO_3$ increased from ~50 nm at 90°C to ~100 nm at 240°C. At synthesis temperatures below ~150°C, the $BaTiO_3$ particles had a narrow size distribution and were predominantly cubic in structure. Higher synthesis temperatures produced a mixture of the cubic and tetragonal phases in which the concentration of the tetragonal phase increased with increasing temperature. A bimodal distribution of sizes developed for long reaction times (96 h) at the highest synthesis temperature (240°C). Thermal analysis revealed little weight loss on heating the powders to temperatures up to 700°C. The influence of particle size and processing-related hydroxyl defects on the crystal structure of the $BaTiO_3$ powder is discussed.

1. Introduction

Barium titanate is an important material in the electronics industry [1–3]. Its high dielectric constant and low dielectric loss factor over a wide range of temperature and frequency make it desirable as a dielectric material for the manufacture of capacitors while its ferroelectric properties are exploited for applications such as piezoelectric transducers. It is also increasingly used as nonlinear resistors with positive temperature coefficients (PTC resistors) for measuring and control applications in the electronic industry. Barium titanate materials are commonly fabricated by a conventional ceramic processing route involving the consolidation and sintering of $BaTiO_3$ powders. The common industrial routes for the preparation of $BaTiO_3$ powders include the calcination of a mixture of $BaCO_3$ and TiO_2 powders at temperatures of 1000–1200°C [4, 5] and the thermal decomposition of barium-titanyl oxalate [$BaTiO(C_2O_4)_2 \cdot 4H_2O$] at temperatures in the range of 800–1100°C [4, 6]. Bonding and agglomeration of the particulate product are common features of these solid state reactions and milling is normally required to achieve particle sizes down to ~1 μm.

The production of thin dielectric layers, particularly for multilayer ceramic capacitors, coupled with improvement in the properties and reliability, require finer $BaTiO_3$ powders with high purity and compositional homogeneity. Recent emphasis has focussed on chemical methods such as precipitation (or coprecipitation) from solution or sol-gel processing [6–9]. However, in most of these solution-based approaches, the product is either an amorphous phase or a precursor compound so that a calcination step at 800–1000°C, followed by milling, is commonly required to form a crystalline $BaTiO_3$ powder with controlled particle size. The calcination and milling steps are similar to those used in the solid state methods so that a significant improvement in the powder quality is normally not achieved.

Hydrothermal synthesis provides an alternative route for the synthesis of fine crystalline oxide powders with controlled characteristics at relatively low temperatures. The process, involving precipitation from solution at temperatures typically between the boiling point and critical point of water (100°C and 374.2°C) in an autoclave, has been used for decades for the synthesis of fine oxide powders [10]. Crystalline $BaTiO_3$ powders have been synthesized at temperatures between ~100–200°C by reacting fine TiO_2 particles with a strongly alkaline solution ($pH > 12$) of $Ba(OH)_2$ [11–17]. Other starting materials, such as $TiCl_4$, titanium alkoxide and TiO_2 gels, have been used as the titanium source at reaction temperatures in the range of 100–400°C [18]. Hydrothermal $BaTiO_3$ powders typically have fine particle sizes in the range of 50–400 nm and a narrow distribution of sizes making these powders highly sinterable as well as attractive for the production of thin dielectric layers.

Hydrothermal $BaTiO_3$ powders show a number of structural characteristics that are not observed for powders prepared by conventional solid state reaction at higher temperatures. X-ray diffraction of hydrothermal $BaTiO_3$ powders, particularly those synthesized

at lower temperatures, reveals a cubic structure that is normally observed only at temperatures above the ferroelectric Curie temperature of 125–130°C. The possible causes for the apparent cubic structure and nonferroelectric properties of fine $BaTiO_3$ particles are not clear and have been discussed elsewhere [19]. They include (i) the idea of a critical size for ferroelectricity arising from factors such as depolarization effects and the absence of long-range cooperative interactions and (ii) particularly for chemically prepared $BaTiO_3$ powders, the presence of a high concentration of charged point defects that might upset the long range polar ordering that drives the cubic to tetragonal structural transformation on cooling. Clustering of fine $BaTiO_3$ particles has also been suggested to have a significant influence on the cubic to tetragonal phase transformation [20].

For hydrothermal $BaTiO_3$ powders (particle size ~200 nm) prepared from acetate precursors, Hennings and Schreinemacher [21] showed that the development of room-temperature tetragonal structure after heat treatment was closely associated with the elimination of hydroxyl defects in the structure and not with particle growth. However, for hydrothermal $BaTiO_3$ prepared from hydrolyzed titanium alkoxide and $Ba(OH)_2$ solution, Begg *et al*. [22] concluded that the cubic to tetragonal structural transformation was not associated with the removal of hydroxyl groups during heating but was essentially dependent only on the particle size. The investigation of sol-gel processed $BaTiO_3$ polycrystals by Frey and Payne [19] indicated that a more complex evolution of subtle structural changes took place. Barium titanate that was cubic in structure according to X-ray diffraction (referred to as XRD-cubic) and free of hydroxyl defects displayed Raman spectra attributed to the orthorhombic phase. Reduction in grain size was found to enhance the stability of the orthorhombic phase at room temperature. Raman activity for XRD-cubic materials appeared not to be associated only with the presence of hydroxyl defects in the structure. Furthermore, the room temperature tetragonal structure appeared not to be tied directly to the removal of the hydroxyl groups. With increasing grain size from 35 to 100 nm, the room temperature XRD patterns and the Raman spectra exhibited the characteristics of the tetragonal phase.

In the present work, the synthesis of hydrothermal $BaTiO_3$ powders by a reaction between fine TiO_2 particles and a strongly alkaline solution of $Ba(OH)_2$ was investigated. The objective was to determine how the synthesis parameters influence the composition and structure of the particles in order to achieve powders with controlled characteristics. Since a distinctive feature of fine $BaTiO_3$ powders is the tendency to exhibit an XRD-cubic structure at room temperature, the relationship of the structure (as determined by XRD) to the size and hydroxyl content for this processing method is reported. However, the work does not attempt to determine a cause for the size effect on the structure.

2. Experimental

Barium titanate powders were synthesized by reacting TiO_2 powder (Degussa Corp., South Planefield, NJ) with an aqueous solution of $Ba(OH)_2$ (pH > 14). The TiO_2 powder, average particle size ≈25 nm, consisted of ~30 weight percent (wt%) rutile and ~70 wt% anatase. In the experiment, 8 g of $Ba(OH)_2 \cdot 8H_2O$ (Aldrich, Milwaukee, WI) was added to 12 cc of deionized water in a Teflon-lined autoclave (45 ml capacity; Parr Instrument Co., Moline, IL). The system was purged with argon, sealed and heated to 80°C until the $Ba(OH)_2 \cdot 8H_2O$ dissolved. Two grams of TiO_2 was then added to the solution, the system was sealed, heated rapidly to the reaction temperature (in the range of 80°C to 240°C) and held for given times (1 to 48 h). After the reaction, the product was washed first with formic acid (~0.1 molar) to remove any residual $BaCO_3$ and then washed with deionized water. The powder was dried in an oven for 24 h at 85°C.

The phase composition, structure and crystallite size of the powders were determined by X-ray diffraction (Scintag XDS 2000) using Cu K_α radiation ($\lambda = 0.15406$ nm) in a step-scan mode ($2\theta = 0.03°$ per step). X-ray diffraction patterns were analyzed using SHADOW and RIQAS software (Materials Data Inc., Livermore, CA) to determine the crystallite size and the concentration of the cubic and tetragonal phases in the powder. The SHADOW and RIQAS pattern analysis programs use a direct convolution method in profile and whole pattern fitting [23]. Refined patterns were used to determine the unit cell dimensions, the line splitting and the crystallite size. The RIQAS software was used for quantitative analysis of each phase in the powders based on the Rietveld structure refinement and whole pattern fitting of X-ray diffraction patterns. The two diffraction lines at 2θ values of 38.9° ($hkl = 111$) and 83.3°($hkl = 222$) were employed in the determination of the crystallite size by X-ray line broadening because they represent the only lines in the tetragonal phase pattern which do not undergo broadening due to line splitting. In the absence of lattice strain, the broadening of these two lines can be attributed only to the crystallite size effect.

The morphology and size of the powders were observed in a transmission electron microscope (Philips EM430T). The average particle size was determined by measuring the maximum diameters of more than 200 particles. Thermal analysis (Netzsch STA 409; Selb, Germany), involving thermogravimetric analysis (TGA) and differential thermal analysis (DTA), was performed by heating the powders (previously dried for 24 h at 85°C) in air at 2°C/min to 1000°C. The elemental composition of the powder was determined by inductively coupled plasma (ICP) atomic emission spectroscopy (Acme Analytical Labs., Vancouver, BC, Canada).

A preliminary examination of the sintering characteristics of the $BaTiO_3$ powder was performed. The powders were compacted uniaxially in a stainless steel die (pressure ≈20 MPa) followed by cold isostatic pressing under a pressure of ~250 MPa to produce pellets (~6 mm in diameter by 4 mm) with a green density of ~0.60 of the theoretical value. The compacts were sintered in air in a dilatometer (1600C, Theta, Port Washington, NY) at a constant heating rate of 10°C per minute to 1350°C.

3. Results

X-ray diffraction of the product revealed that the hydrothermal synthesis reaction proceeded fairly rapidly. Considerable $BaTiO_3$ powder was formed after only 1 h of reaction at 150°C (Fig. 1). Rietveld analysis showed that the product consisted of 92.5 wt% cubic $BaTiO_3$ with an estimated standard deviation (ESD) of 1.1 wt% and ~7.5 wt% unreacted TiO_2 (rutile) with an ESD of 0.8 wt%. After 12 h, X-ray diffraction revealed only cubic $BaTiO_3$ in the product. Prolonging the reaction time to 48 h produced a mixture consisting of 94.7 wt% cubic phase (ESD = 1.0 wt%) and 5.3 wt% tetragonal phase (ESD = 0.9 wt%).

The synthesis of $BaTiO_3$ was also investigated as a function of the reaction temperature for a fixed time of 24 h. X-ray diffraction revealed that the powders synthesized at temperatures below 100°C contained a small concentration of unreacted TiO_2 but above this temperature, the product consisted of $BaTiO_3$ only. Furthermore, at lower reaction temperatures (below ~150°C), the powders were predominantly cubic while at higher temperatures, the formation of the tetragonal phase started to become significant (concentration greater than ~10 wt%). However, even at the highest synthesis temperature (240°C), complete formation of the tetragonal phase was not achieved. At this temperature, the concentration of tetragonal $BaTiO_3$ was only ~30 wt%. Table I summarizes the phase composition, as determined by Rietveld analysis, for the powders produced after 24 h at various reaction temperatures. The concentrations of the cubic and tetragonal phases in the product are plotted as a function of temperature in Fig. 2.

The phase composition of the $BaTiO_3$ powders as function of reaction time at 240°C (the highest reaction temperature) was also determined by Rietveld analysis. The concentration of the tetragonal phase increases slowly from 29.2 wt% (ESD = 0.2 wt%) for a reaction time of 24 h to 40.6 wt% (ESD = 0.9 wt%) after 96 h of reaction (Table II and Fig. 3).

The splitting of the X-ray diffraction peak at ~45° 2θ ($hkl = 200$), indicative of the presence of tetragonal

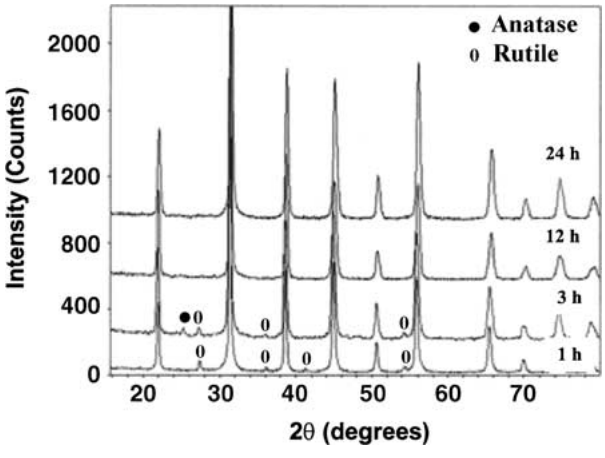

Figure 1 X-ray diffraction patterns of $BaTiO_3$ powders synthesized for given times at 150°C by reacting fine TiO_2 particles with a strongly alkaline solution of $Ba(OH)_2$.

TABLE I Phase composition of hydrothermal $BaTiO_3$ powders produced after 24 hours at various reaction temperatures

Reaction temperature (°C)	Phases identified	Concentration wt%	Concentration standard, deviation (ESD)
80	Cubic $BaTiO_3$	90.0	1.1
	Tetragonal $BaTiO_3$	1.1	0.2
	Unreacted TiO_2	8.9	0.4
90	Cubic $BaTiO_3$	88.6	1.8
	Tetragonal $BaTiO_3$	5.2	0.3
	Unreacted TiO_2	6.2	0.6
100	Cubic $BaTiO_3$	95.8	1.2
	Tetragonal $BaTiO_3$	2.3	0.2
	Unreacted TiO_2	1.9	0.4
120	Cubic $BaTiO_3$	91.2	1.6
	Tetragonal $BaTiO_3$	8.8	0.9
140	Cubic $BaTiO_3$	94.4	1.8
	Tetragonal $BaTiO_3$	5.6	0.9
160	Cubic $BaTiO_3$	93.5	1.0
	Tetragonal $BaTiO_3$	6.5	0.2
180	Cubic $BaTiO_3$	86.0	0.9
	Tetragonal $BaTiO_3$	14.0	0.1
200	Cubic $BaTiO_3$	74.9	1.3
	Tetragonal $BaTiO_3$	25.1	0.7
220	Cubic $BaTiO_3$	76.8	1.9
	Tetragonal $BaTiO_3$	23.2	0.1
240	Cubic $BaTiO_3$	70.8	1.2
	Tetragonal $BaTiO_3$	29.2	0.2

TABLE II Phase composition of hydrothermal $BaTiO_3$ powders produced after various reaction times at 240°C

Reaction time, (h)	Phases identified	Concentration (wt%)	Estimated standard deviation (ESD)
24	Cubic $BaTiO_3$	70.8	1.2
	Tetragonal $BaTiO_3$	29.2	0.2
48	Cubic $BaTiO_3$	66.5	1.7
	Tetragonal $BaTiO_3$	33.5	0.5
72	Cubic $BaTiO_3$	56.5	1.0
	Tetragonal $BaTiO_3$	43.5	0.3
96	Cubic $BaTiO_3$	59.4	0.7
	Tetragonal $BaTiO_3$	40.6	0.9

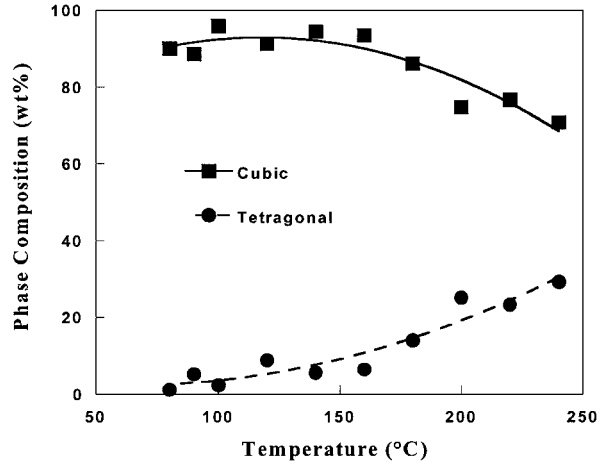

Figure 2 Concentration of the cubic and tetragonal phases determined by Rietveld analysis for $BaTiO_3$ powders synthesized for 24 h at different temperatures.

$BaTiO_3$, is shown in Fig. 4 for the powders formed after 24 h of reaction at several representative temperatures. (The patterns for the powders produced at the other reaction temperatures are omitted to maintain clarity of

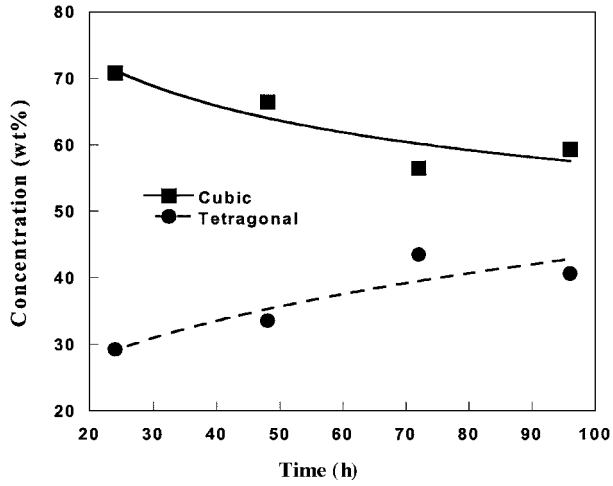

Figure 3 Concentration of the cubic and tetragonal phase determined by Rietveld analysis for $BaTiO_3$ powders synthesized for 24 to 96 h at 240°C.

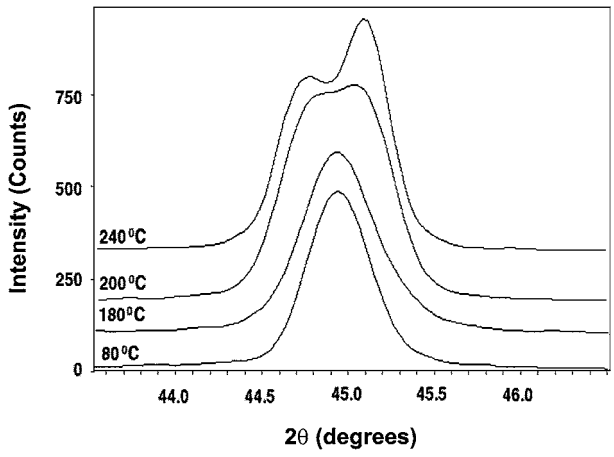

Figure 4 X-ray diffraction patterns of $BaTiO_3$ powder synthesized for 24 h at different temperatures showing peak splitting above 180°C due to increasing concentration of the tetragonal phase.

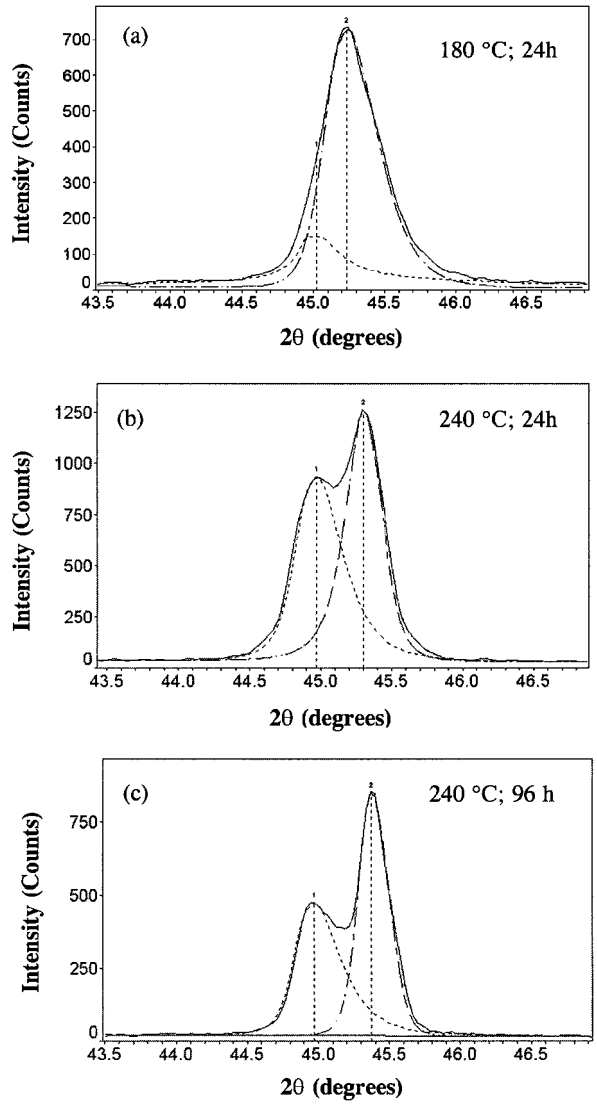

Figure 5 Experimental and deconvoluted patterns (determined by SHADOW software) for the X-ray peaks at $2\theta \approx 45°$ ($hkl = 200$) for $BaTiO_3$ powders synthesized under different conditions, showing the extent of splitting between the peaks.

the figure.) The peak splitting starts to become clear at 200°C. At this temperature, Rietveld analysis (Table I and Fig. 2) indicates that the tetragonal content is already ~20 wt%.

SHADOW software was used to deconvolute the spectrum at ~45° 2θ ($hkl = 200$) into two separate peaks, and the magnitude of the peak splitting (taken as the difference in 2θ value between the two peaks) was determined. Fig. 5 shows examples of the experimental and deconvoluted peaks for $BaTiO_3$ powders synthesized for 24 h at 150°C and 240°C and for 96 h at 240°C. For powders synthesized for a fixed reaction time of 24 h, Fig. 6 shows that the magnitude of the splitting first increases with the synthesis temperature but then flattens out to a value of 0.35–0.37° for synthesis temperatures above 200°C.

Fig. 7 shows TEM micrographs of the $BaTiO_3$ powders produced after 24 h of reaction at 90°C, 160°C and 240°C, and after 96 h at 240°C. At lower temperatures [Fig. 7a and b], the particles appear to have a fairly narrow size distribution. Coarser faceted particles are apparent in the powder synthesized at 240°C and a bimodal distribution of larger faceted particles

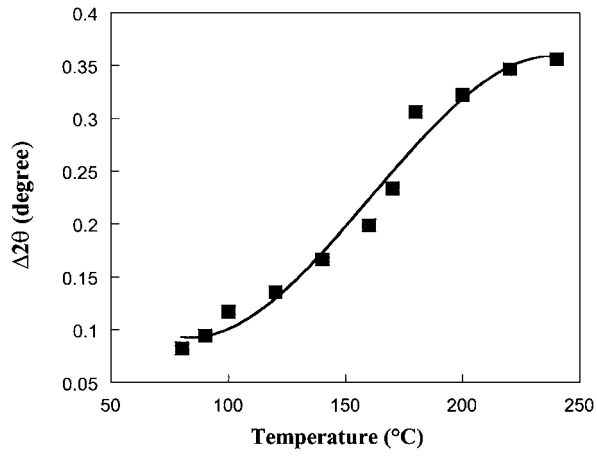

Figure 6 Data for the peak splitting of the X-ray lines at $2\theta \approx 45°$ ($hkl = 200$) for $BaTiO_3$ powders synthesized for 24 h at different temperatures.

and smaller particles is clearly observed for the powders synthesized for 96 h at 240°C.

The data for the average crystallite size (determined by X-ray line broadening) and the average particle size

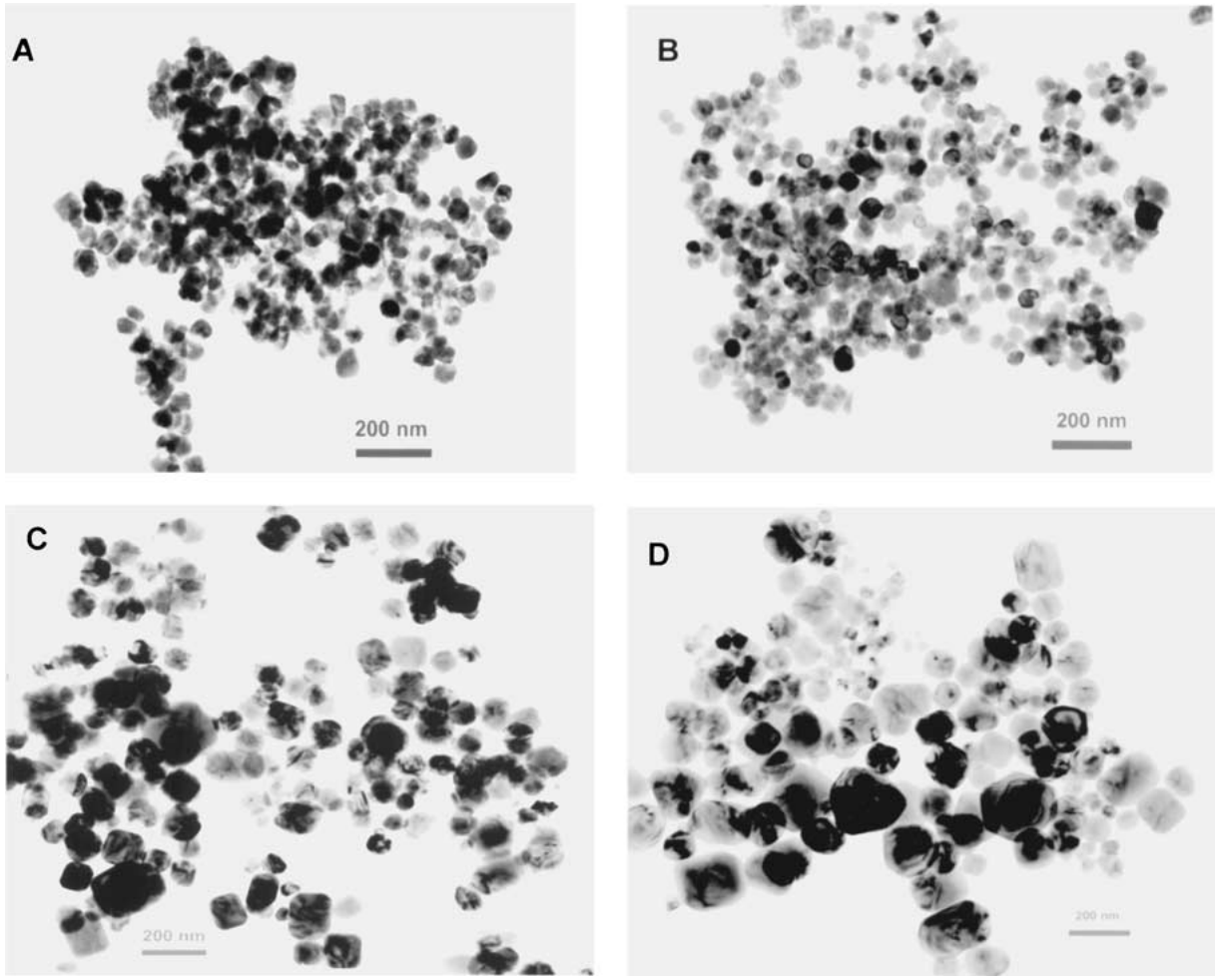

Figure 7 Transmission electron micrographs of $BaTiO_3$ powders synthesized for 24 h at 90°C (A), 160°C (B), and 240°C and for 96 h at 240°C (D).

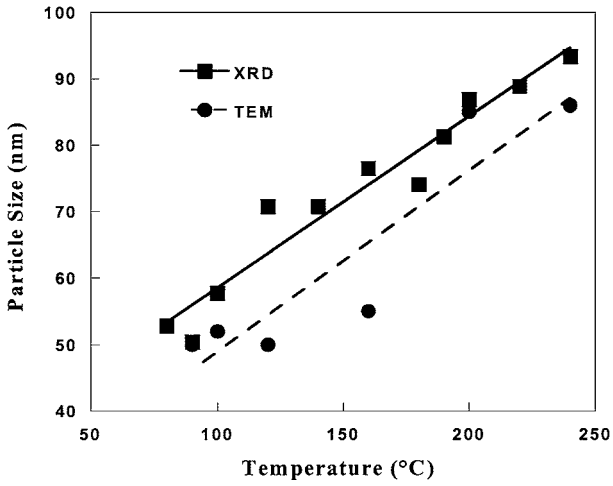

Figure 8 Average particle size for $BaTiO_3$ powders synthesized for 24 h at different temperatures, as determined by X-ray line broadening and transmission electron microscopy.

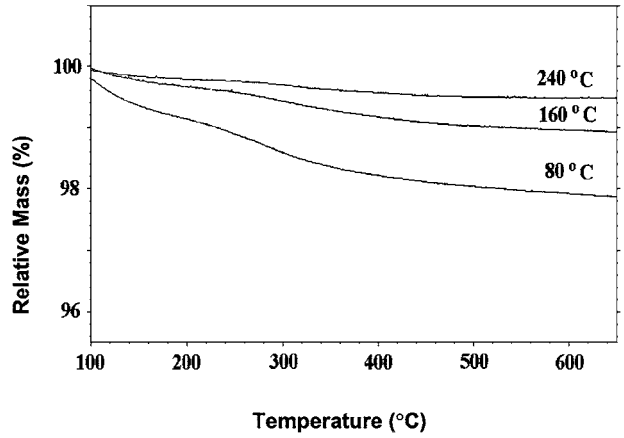

Figure 9 Thermogravimetric analysis of $BaTiO_3$ powders synthesized for 24 h at 80°C, 160°C, and 240°C showing the weigh loss during heating in air at 2°C/min to 700°C.

(determined by TEM) for $BaTiO_3$ powders formed after 24 h of reaction at temperatures between 80°C and 240°C, are shown in Fig. 8. The data obtained by the two methods agree to within ±10%. They show an increase in the average crystallite (or particle) size from ∼50 nm at 80°C to ∼100 nm at 240°C.

Fig. 9 shows the data for the weight loss as a function of temperature during TGA analysis for $BaTiO_3$ powders produced after 24 h of reaction at 80°C, 160°C and 240°C. The total weight loss between 100°C and 600°C is <2 wt% for the powder synthesized at 80°C and decreases significantly with increasing temperature of synthesis, becoming <0.5 wt% at 240°C. The total weight loss consists of two contributions: one from residual, physically adsorbed water which may be responsible for the weight loss below ∼200°C and the other from chemically bound hydroxyl groups that

TABLE III Ba:Ti elemental ratio for the $BaTiO_3$ powders synthesized for 24 h at various temperatures

Synthesis temperature (°C)	BaO content (wt%)	TiO_2 content (wt%)	Ba:Ti ratio
100	56.27	35.96	0.90
160	55.28	37.03	0.96
200	57.58	34.45	0.99
240	58.17	33.92	0.99

are commonly decomposed in the range of ∼200°C to 500°C. From Fig. 9, the weight loss in the range of 200°C to 500°C is found to be 1.2%, 0.6% and 0.4% for the powders synthesized at 80°C, 160°C and 240°C, respectively.

The Ba/Ti elemental ratio for the powders produced after 24 h of reaction at different temperatures was determined by atomic emission spectroscopy and the data are summarized in Table III for four representative temperatures. At lower reaction temperatures (e.g., 100°C), the ratio is relatively low (e.g., 0.90) but at temperatures above ∼200°C, the ratio (0.99) is very close to the stoichiometric value of 1.0. Three factors may be responsible for the low Ba/Ti elemental ratio found for the powders prepared at lower temperatures. First, incomplete reaction leads to the presence unreacted TiO_2 in the product. Rietveld analysis (Table I) showed the presence of 1.9 wt% TiO_2 in the powder produced at 100°C. Taking this concentration of unreacted TiO_2 into account, the Ba/Ti ratio is expected to be 0.94. Second, as a result of the nucleation and growth mechanism for the $BaTiO_3$ particles (discussed later), it is possible that a small amount of unreacted TiO_2 might be encapsulated within the $BaTiO_3$ particles. While this encapsulated TiO_2 may not be detectable by X-ray analysis, it will lead to a reduction of the Ba/Ti ration as determined by atomic emission spectroscopy. Third, washing the prepared powder with formic acid or water leads to decomposition of $BaTiO_3$ to $Ba(OH)_2$ (which remains in solution), and TiO_2 (which, presumably is amorphous). The extent of the reaction depends on the particle size, the temperature, and the time. While the washing step was carried out at room temperature for relatively short times, the finer particles prepared at 100°C are more soluble than those prepared at 240°C, so a higher concentration of TiO_2 might be expected in the powder prepared at 100°C. This higher TiO_2 content results in a reduction in the Ba:Ti ratio.

Fig. 10 shows the sintering kinetics of compacts formed from $BaTiO_3$ powders synthesized at 120°C and 240°C. Powders synthesized above 100°C do not show significant differences in sintering kinetics and the curves for the other synthesis temperatures have been omitted to preserve clarity of the figure. The final density of the sintered compacts was greater than 95% of the theoretical density of $BaTiO_3$. For powder synthesis temperatures below 100°C, the final density of the sintered compacts was significantly lower (∼75 of the theoretical density). A scanning electron micrograph of the polished surface of a sintered compact (prepared from a powder synthesized at 120°C) is shown

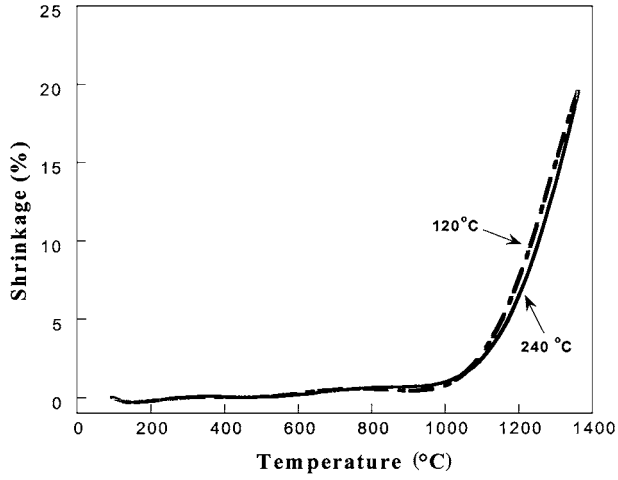

Figure 10 Sintering behavior of $BaTiO_3$ compacts formed from the powder synthesized at 120°C and 240°C during constant heating rate sintering at 10°C/min to 1350°C.

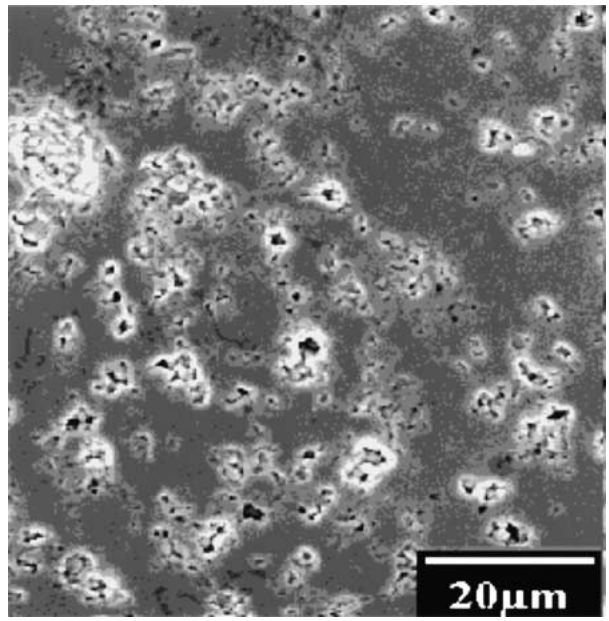

Figure 11 Scanning electron micrograph of the polished surface of a sintered $BaTiO_3$ pellet formed from the powder synthesized at 120°C and sintered at 10°C/min to 1350°C.

in Fig. 11. They show highly dense regions and isolated regions of large pores resulting presumably from inhomogeneous packing of the fine powders.

4. Discussion

The reaction conditions employed in the hydrothermal synthesis experiments are consistent with thermodynamic predictions for the Ti-Ba-H_2O system [24] which indicate that $BaTiO_3$ is the thermodynamically favored phase at pH values greater than 12 and for high Ba^{2+} concentration (2 molar). Similar reaction conditions of pH and Ba^{2+} concentration were employed by Chien *et al*. [16] for the synthesis of $BaTiO_3$ particles at ambient pressure and temperatures less than 100°C. Based on these experiments, the thermodynamic foundation for the formation of $BaTiO_3$ appears reasonably established.

The mechanism of nucleation and growth of $BaTiO_3$ particles is not clear. Hertl [25] assumed that the TiO_2 particles react initially with the dissolved Ba^{2+} ions, thereby producing a continuous layer of $BaTiO_3$ through which the additional Ba^{2+} ions must diffuse for the reaction to continue. The $BaTiO_3$ layer may provide an effective diffusion barrier that serves to slow or ultimately halt the reaction. Another mechanism involves a dissolution/precipitation process in which Ti is hydrolyzed to form either $Ti(OH)_6^{2-}$ [26] or $Ti(OH)_4$ [27], followed by subsequent reaction with Ba^{2+} ions to precipitate $BaTiO_3$. In this case, nucleation of $BaTiO_3$ may occur heterogeneously on the TiO_2 reactant particles or homogeneously in the solution. When heterogeneous necleation occurs, it is possible for the TiO_2 reactant particle to become encapsulated, and this also serves to limit the reaction rate. The fine TiO_2 particles used in the present work can provide efficient sites for heterogeneous nucleation, as observed by Chien *et al.* [16].

Mechanisms for subsequent growth of the $BaTiO_3$ particles include the classical "growth by diffusion" mechanism in which additional matter diffuses through the liquid and precipitates on the existing particles [28], aggregation of the particles to form clusters [29, 30], and Ostwald ripening in which the smaller particles dissolve and precipitate on the larger particles [31–33]. For crystalline particles synthesized under hydrothermal conditions, growth by aggregation may be possible in the early stages. However, the hydrothermal particles are commonly observed to be single crystals [34, 35], and therefore aggregation cannot play a significant role after the early stages.

The data indicate that the reaction time for the formation of $BaTiO_3$ is quite short: essentially single phase $BaTiO_3$ after only ~1 h at a reaction temperature of ~150°C (Fig. 1). This reaction time will increase somewhat at lower temperatures and will decrease at higher temperatures. Since the total reaction time at each temperature was 24 h, the system for the most part of the synthesis process can be considered to consist of a dilute suspension of $BaTiO_3$ particles. Coarsening by Ostwald ripening is expected to be the dominant particle growth process. For the predominantly single-phase (cubic) particles produced at reaction temperatures below ~180°C [Fig. 7a and b], particles with a narrow distribution of sizes are produced. However, at higher reaction temperatures, the appearance of the tetragonal phase produces a broadening of the overall distribution [Fig. 7c] and eventually a bimodal distribution for prolonged reaction times [Fig. 7d].

According to Fig. 8, the average particle size increases with an increase in the reaction temperature. It would be expected that the fraction of particles above some given size would also increase with increasing size. It is also observed from Fig. 4 that the concentration of tetragonal $BaTiO_3$ particles increases with increasing temperature. The data of Figs 4 and 8 are therefore consistent with the idea of a critical size for ferroelectricity.

As outlined earlier, Hennings and Schreinemacher [21] have suggested that the room temperature cubic structure of hydrothermal $BaTiO_3$ particles is associated with the presence of hydroxyl defects in the $BaTiO_3$ structure. They observed weight loss values of ~1.5% in the temperature range of 200°C to 500°C for hydrothermal powders prepared from barium titanium acetate precursors [36]. In the same decomposition temperature range, the weight loss observed in the present work are smaller, with the values decreasing from 1.2% to 0.4% for the powders synthesized at 80°C and 240°C, respectively (Fig. 9). Since the average particle size in the present work increased by a factor of ~2 when the powder synthesis temperature increased from 80°C to 240°C, then the change in the weight loss values with the powder synthesis temperature can be accounted for mostly by the reduction in surface area. If the differences in surface hydroxyl content due to differences in surface area are corrected for, little change in the phase composition of the $BaTiO_3$ product is expected in the present experiments for the powders synthesized at different temperatures. However, the X-ray analysis data (Fig. 4) show that the concentration of tetragonal $BaTiO_3$ in the product increased with the synthesis temperature, reaching a value of ~30 wt% at 240°C. It appears, therefore, that the room temperature X-ray diffraction structure data obtained for the present hydrothermal powders cannot be well explained solely by the presence of hydroxyl defects in the $BaTiO_3$ structure.

5. Conclusions

Hydrothermal $BaTiO_3$ powders synthesized by reacting fine TiO_2 particles with a strongly alkaline solution of $Ba(OH)_2$ for 24 h have a room temperature cubic structure by X-ray analysis when the reaction temperature is below ~150°C. Powders synthesized above this temperature have a mixture of the cubic and tetragonal phases, with the content of the tetragonal phase increasing with increasing reaction temperature. The average particle size increased from ~50 nm to ~100 nm when the reaction temperature was increased from 80°C to 240°C. Between 200°C and 500°C, commonly the temperature range for decomposition of hydroxyl groups, the weight loss of the powders was relatively small and also decreased as the synthesis temperature of the powders increased. The room temperature X-ray diffraction structure of the powders appears to be consistent with a critical size for ferroelectricity and cannot be well explained by the presence of hydroxyl defects in the $BaTiO_3$ structure.

References

1. L. E. CROSS, *Am. Ceram. Soc. Bull.* **63** (1984) 586.
2. D. HENNINGS, *Int. J. High Tech. Ceram.* **3** (1987) 91.
3. R. E. NEWNHAN, *Rept. Prog. Phys.* **52** (1989) 123.
4. M. S. H. CHU and A. W. I. M. RAE, *Am. Ceram. Soc. Bull.* **74** (1995) 69.
5. A. BAUGER, J. C. MUTIN and J. C. NIEPCE, *J. Mater. Sci.* **18** (1983) 3041; **18** (1983) 3543.
6. D. HENNINGS, in "British Ceramic Society Proceedings," Vol. 41: Electroceramics, edited by A. I. Moulson, J. Binner and R. Morrell (The Institute of Ceramics, Stoke-on-Trent, UK, 1989) p. 1.

7. F. CHAPUT and J. P. BOILOT, *J. Amer. Ceram. Soc.* **73** (1990) 942.
8. D. HENNINGS and W. MAYR, J. *Solid State Chem.* **26** (1978) 329.
9. P. P. PHULE and S. H. RISBUD, *J. Mater. Sci.* **25** (1990) 1169.
10. W. J. DAWSON, *Am. Ceram. Soc. Bull.* **67** (1988) 1673.
11. J. H. PETERSON, U.S. Patent No. 2216655 (October 22, 1940).
12. A. N. CHRISTENSEN and S. E.RASMUSSEN, *Acta Chem. Scand.* **17** (1963) 845.
13. T. KUBO, M. KATO and T. FUGITA, *Kogyo Kagaku Zasshi* **71** (1968) 114.
14. H. YAMAMURA, S. SHIRASAKI, K. TAKAHASHI and M. TAGAKI, *Nippon Kagaku Kaishi* **7** (1974) 1155.
15. A. N. CHRISTENSEN, *Acta Chem. Scand.* **24** (1970) 2447.
16. A. T. CHIEN, J. S. SPECK, F. F. LANGE, A. C. DAYKIN and C. G. LEVI, *J. Mater. Res.* **10** (1995) 1784.
17. J. O. ECKERT, JR., C. C. HUNG-HOUSTON, B. L. GERSTEN, M. M. LENCKA and R. E. RIMAN, *J. Amer. Ceram. Soc.* **79** (1996) 2929.
18. R. VIVEKANANDAN and T. R. N. KUTTY, *Powder Technol.* **57** (1989) 181.
19. M. H. FREY and D. A. PAYNE, *Phys. Rev.* **54** (1996) 3158.
20. X. LI and W.-H. SHIH, *J. Amer. Ceram. Soc.* **80** (1997) 2844.
21. D. HENNINGS and S. SCHREINEMACHER, *J. Europ. Ceram. Soc.* **9** (1992) 41.
22. B. D. BEGG, E. R. VANCE and J. NOWOTNY, *J. Amer. Ceram. Soc.* **77** (1994) 3186.
23. S. A. HOWARD and R. L. SNYDER, *J. Appl. Cryst.* **22** (1989) 238.
24. K. OSSEO-ASARE, F. J. ARRIAGADA and J. H. ADAIR, *Ceramic Trans.* **1** (1988) 47.
25. W. HERTL, *J. Amer. Ceram. Soc.* **71** (1988) 879.
26. M. YOSHIMURA, S.-E. YOO, M. HAYASHI and N. ISHIZAWA, *Jpn. J. Appl. Phys.* **28** (1989) 2007.
27. R. BACSA, P. RAVINDRANATHAN and J. P. DOUGHERTY, *J. Mater. Res.* **7** (1992) 423.
28. V. K. LAMER and R. H. DINEGAR, *J. Am. Chem. Soc.* **72** (1950) 4847.
29. E. MATIJEVIC, *Langmuir* **4** (1988) 31.
30. G. H. BOGUSH, G. L. DICKSTEIN, K. C. LEE and C. F. ZUKOSKI, *Mater. Res. Soc. Symp. Proc.* **121** (1988) 57.
31. G. W. GREENWOOD, *Acta Metall.* **4** (1956) 243.
32. C. WAGNER, *Z. Electrochem.* **65** (1961) 581.
33. I. M. LIFSHITZ and V. V. SLYOZOV, *J. Phys. Chem. Solids* **19** (1961) 35.
34. S. LAKHWANI and M. N. RAHAMAN, *J. Mater. Res.* **14** (1999) 1455.
35. M. N. RAHAMAN and Y. C. ZHOU, *J. Europ. Ceram. Soc.* **15** (1995) 939.
36. D. HENNINGS, G. ROSENSTEIN and H. SCHREINEMACHER, *J. Europ. Ceram. Soc.* **8** (1991) 107.

Received 8 November 2000
and accepted 13 July 2001